

8-20-2024

Synthesis and photooxygenation of 3-(p-substituted phenyl)-3a,8a-dihydro-4H-cyclohepta[d]isoxazoles: Facial selectivity

MAHİRE EMEL OLGUN

ABDULLAH MENZEK

ERTAN ŞAHİN

YASİN ÇETİNKAYA

Follow this and additional works at: <https://journals.tubitak.gov.tr/chem>

 Part of the [Chemistry Commons](#)

Recommended Citation

OLGUN, MAHİRE EMEL; MENZEK, ABDULLAH; ŞAHİN, ERTAN; and ÇETİNKAYA, YASİN (2024) "Synthesis and photooxygenation of 3-(p-substituted phenyl)-3a,8a-dihydro-4H-cyclohepta[d]isoxazoles: Facial selectivity," *Turkish Journal of Chemistry*. Vol. 48: No. 4, Article 13. <https://doi.org/10.55730/1300-0527.3688>





Available at: <https://journals.tubitak.gov.tr/chem/vol48/iss4/13>



This work is licensed under a [Creative Commons Attribution 4.0 International License](#).

This Research Article is brought to you for free and open access by TÜBİTAK Academic Journals. It has been accepted for inclusion in Turkish Journal of Chemistry by an authorized editor of TÜBİTAK Academic Journals. For more information, please contact pinar.dundar@tubitak.gov.tr.

Synthesis and photooxygenation of 3-(*p*-substituted phenyl)-3a,8a-dihydro-4*H*-cyclohepta[*d*]isoxazoles: facial selectivity

Mahire Emel OLGUN¹ , Abdullah MENZEK^{1,2,*} , Ertan ŞAHİN¹ , Yasin ÇETİNKAYA^{1,*} 

¹Department of Chemistry, Faculty of Science, Atatürk University, Erzurum, Türkiye

²Department of Emergency Aid and Disaster Management, Faculty of Health Sciences, Ardahan University, Ardahan, Türkiye

Received: 23.04.2024 • Accepted/Published Online: 28.05.2024 • Final Version: 20.08.2024

Abstract: Two 3-(*p*-substituted phenyl)-3a,8a-dihydro-4*H*-cyclohepta[*d*]isoxazoles were synthesized by 1,3-dipolar cycloaddition of the corresponding nitrile oxides with cycloheptatriene. Two endoperoxides were synthesized as facially selective and single products in high yields (93%–95%) from the reactions of isoxazole derivatives with singlet oxygen. The exact configurations of the endoperoxide with a methyl group in the phenyl ring and the diol synthesized from it were confirmed by X-ray analysis. To elucidate the mechanism, the formation energy of the endoperoxide was investigated by simulations using the software package Gaussian 09 and density functional theory calculations via the M06-2X/6-311+G(d,p) level method in dichloromethane. The results were consistent with experimental findings showing the formation of isoxazole products.

Key words: Diels–Alder reaction, facial selectivity, isoxazole, photooxygenation, density functional theory

1. Introduction

Molecules containing halogen and oxygen derivatives such as hydroxyl, ether, peroxide, and epoxide are important because they can be considered target and intermediate products. Peroxide groups in molecules are generally obtained as unsaturated endoperoxides as a result of cycloaddition reactions of dienes with singlet oxygen [1,2]. The groups in the rings of unsaturated endoperoxides in the structure **1**, where R is Cl and OSiC(CH₃)₃, are in *cis*-configuration, and these endoperoxides are formed as the main product in the reactions of the relevant dienes with singlet oxygen [3,4]. The double bonds in the [2.2.1] and [2.2.2] skeleton structures are stressed due to pyramidization and therefore show dienophile properties in cycloaddition reactions [5–8]. Endoperoxides in the structure **2**, *endo* and *exo*, were formed by the 1,3-dipolar cycloaddition of the corresponding unsaturated endoperoxide and nitrile oxide [9]. The known compound **3** [10] is a bicyclic isoxazole compound and has a conjugated diene structure in its seven-membered ring (Figure 1).

Compound **3** or its derivatives, having isoxazole and cycloheptadiene rings, can be photooxidized. Selectivity can be observed in the formation of these unsaturated endoperoxides and these products will contain three oxygen atoms and one nitrogen atom. Additionally, these products can also be converted into derivatives such as diols. Therefore, these products and reactions are important. For this reason, compounds with Me and OMe were synthesized in the para position of the phenyl ring in the compound **3** structure, and their photooxygenation reactions were examined. It was observed that endoperoxides were formed as single products in high yields in the reaction of isoxazole derivatives with singlet oxygen. To determine the configuration and formation of adducts, some computational studies (e.g., density functional theory (DFT)) were performed.

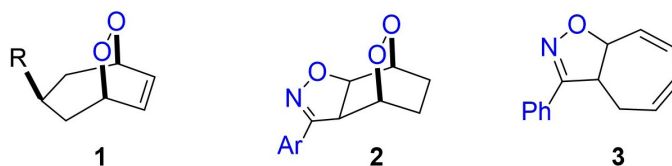


Figure 1. Important diene and endoperoxides.

* Correspondence: abmenzek@ardahan.edu.tr, yasin.cetinkaya@atauni.edu.tr

2. Results and discussion

2.1. Synthesis

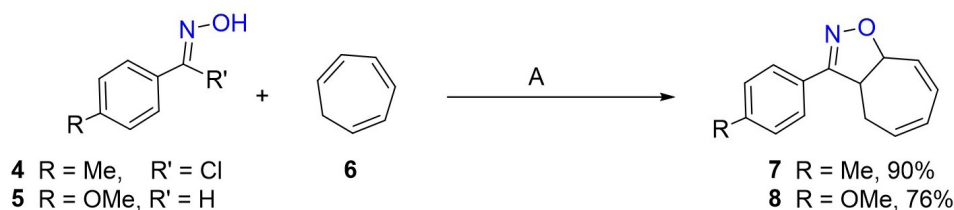
As described previously [7,11,12], oximes **4** and **5** were synthesized to obtain new compounds that are derivatives of compound **3**. Therefore, the reactions of oximes **4** and **5** with cycloheptatriene (CHT) were carried out separately (Scheme 1). The products **7** and **8** obtained from each reaction were purified by column chromatography and obtained in high yields. Adducts **7** and **8** are structures in which five- and seven-membered rings are interlocked with each other. According to the ¹H-NMR spectra of these products, the double bonds in the seven-membered rings were conjugated.

Reactions such as Diels–Alder reactions can be performed with the conjugated diene in the seven-membered ring of compounds **7** and **8** and compounds with various functional groups, especially in its seven-membered ring, can be obtained. As a result of Diels–Alder reactions of conjugated dienes with singlet oxygen and PTAD (4-phenyl-1,2,4-triazoline-3,5-dione), oxygen and nitrogen atoms are placed at the 1,4 positions of the diene [1,2,13,14]. Compound **7** was reacted with both singlet oxygen and PTAD. Only one product from each of these reactions was isolated in high yield (Scheme 2). Since it is understood from their NMR spectra that there is only a double bond in their seven-membered ring, these products are adducts formed by Diels–Alder reactions.

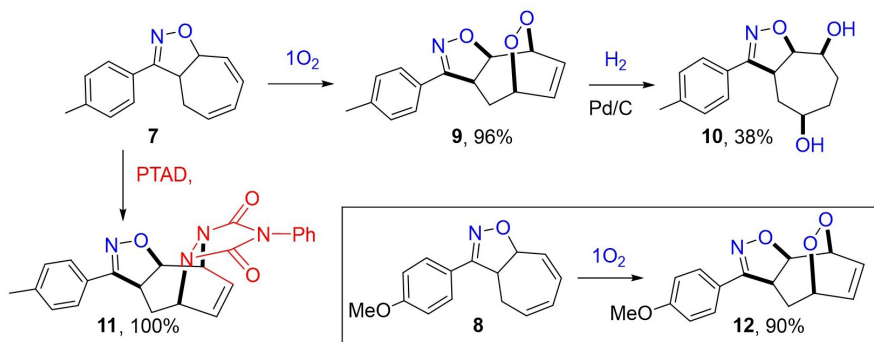
A catalytic hydrogenation reaction is used in the reduction of many functional groups such as unsaturated endoperoxides [1,15–17]. The adduct, endoperoxide **9**, was reacted with gaseous hydrogen (approximately 1.0 atm) in the presence of catalyst Pd/C at room temperature (RT) (Scheme 2). A product was obtained from the purification process of the reaction mixture on the silica gel column chromatography. This product should be a diol derivative because no double bond was present in its seven-membered ring when its NMR spectra were investigated and it was more polar than the corresponding endoperoxide. X-ray analysis of the diol derivative both explains its configuration as **10** and suggests that the structures of the adducts formed from the reactions of **7** with singlet oxygen and PTAD should be **9** and **11**, respectively. Moreover, the proposed structure of endoperoxide **9** was confirmed by X-ray analysis of it.

The exact conformation and structures of (3aS*,5S*,8S*,8aR*)-3-(4-methoxyphenyl)-3a,5,8,8a-tetrahydro-4H-5,8-epidioxycyclohepta[d]isoxazole (**9**) and (3aS*,5R*,8S*,8aR*)-3-(p-tolyl)-3a,5,6,7,8,8a-hexahydro-4H-cyclohepta[d]isoxazole-5,8-diol (**10**) were confirmed by X-ray diffraction analysis. Both solved molecules are in racemic form, and only one enantiomer is seen in the asymmetric unit (Figures 2 and 3). Molecule **9** was crystallized in the orthorhombic Iba2 space group. It consists of fused cycloheptene and heterocyclic oxazole rings with toluene and endoperoxide moiety. Here the cycloheptene ring is in the boat conformation and stressed by the endoperoxide. In the cycloheptene cycle, the length of the C11–C12 double bond is 1.333(3) Å, while the single bonds in the rest of the ring are in the range of 1.483–1.557(3) Å. Moreover, the O2–O3 length of peroxide is 1.461(3) Å and the N1–C7 double bond in the oxazole ring is 1.293(3) Å. For this structure, there is a C13–H...O2 interaction [*D*...*A*=3.168(3) Å] between consecutive enantiomers. The racemic nature of the structures significantly affects the supramolecular structures and crystal lattice motifs (Figure 2).

The other molecule **10** crystallizes in the monoclinic space group P2₁/c with four molecules in the unit cell. The molecule consists of fused cycloheptane and heterocyclic oxazole rings with diol and toluene units. The seven-membered cycloheptane ring adopts a twist-chair conformation. The dihedral angle between the mean planes of the cycloheptane (C8/C14/C10/C11) and oxazole (O3/N1/C7/C8) rings is 29.8°. The C–C (cycloheptane) bond lengths are in the range of 1.516(3)–1.533(3) Å; all have a single bond character. Diol C1–O1 and C2–O2 single bonds are 1.433 Å and 1.420 Å in length, respectively. The N=C double bond in the oxazole ring is quite short (1.278 Å). The molecule forms a consecutive tetramer chain structure with O1–H...O2 [*D*...*A*=2.739(3) Å] and O2–H...O1 [*D*...*A*=2.789(3) Å] hydrogen bonds (Figure 3). The C–H–π interaction [*X*...*Cg* 3.691 Å, *Cg*; Center of gravity of C1/C6 phenyl ring] can be regarded as an important intermolecular interaction in the structure.



Scheme 1. Synthesis of compounds **7** and **8**. A (NEt₃, CH₂Cl₂, –5 °C to RT, 2 days for **7**), (Cold aqueous NaOCl, CH₂Cl₂, –5 °C to RT, 3 days for **8**).



Scheme 2. Reactions of compounds 7 and 8.

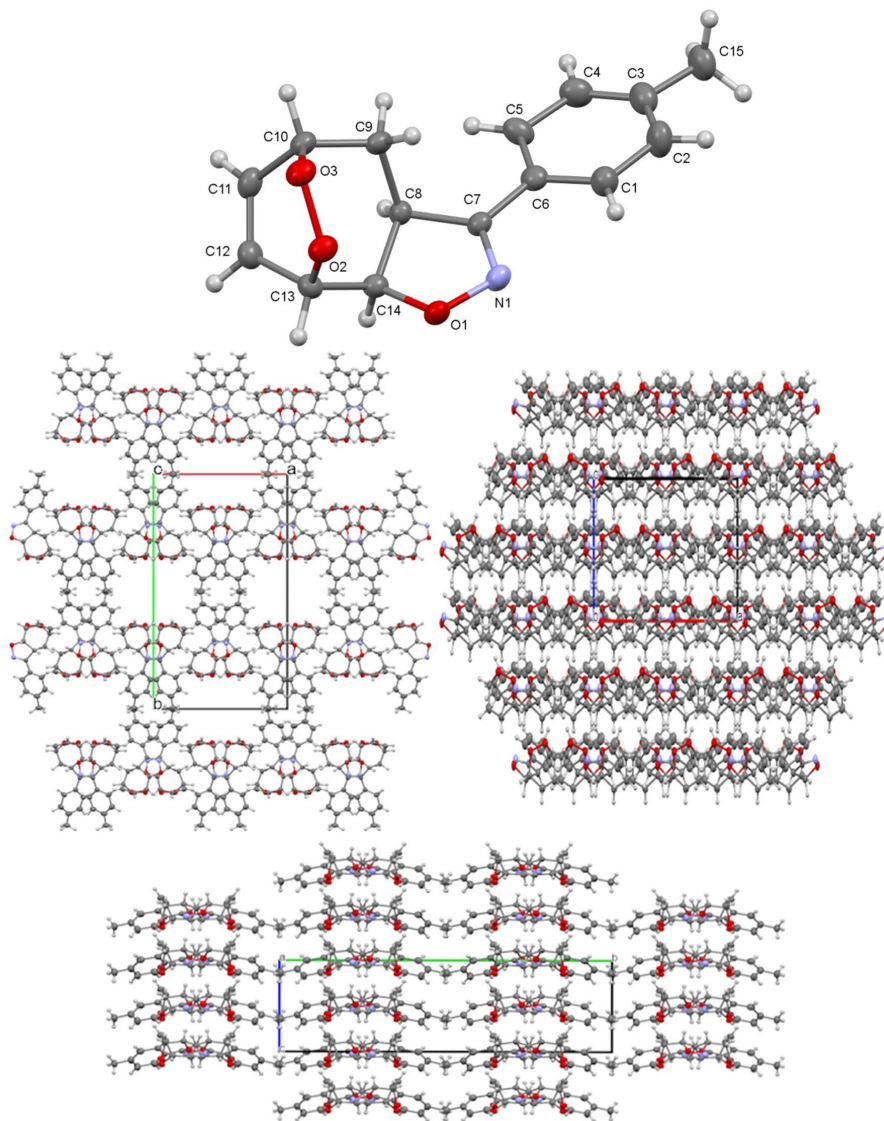


Figure 2. (Top) X-ray structure of the molecule 9. Thermal ellipsoids are drawn at the 40% probability level. (Bottom) The crystal lattice and the unit cell viewed down along the c -, b -, and a -axis, respectively, with the square void motif.

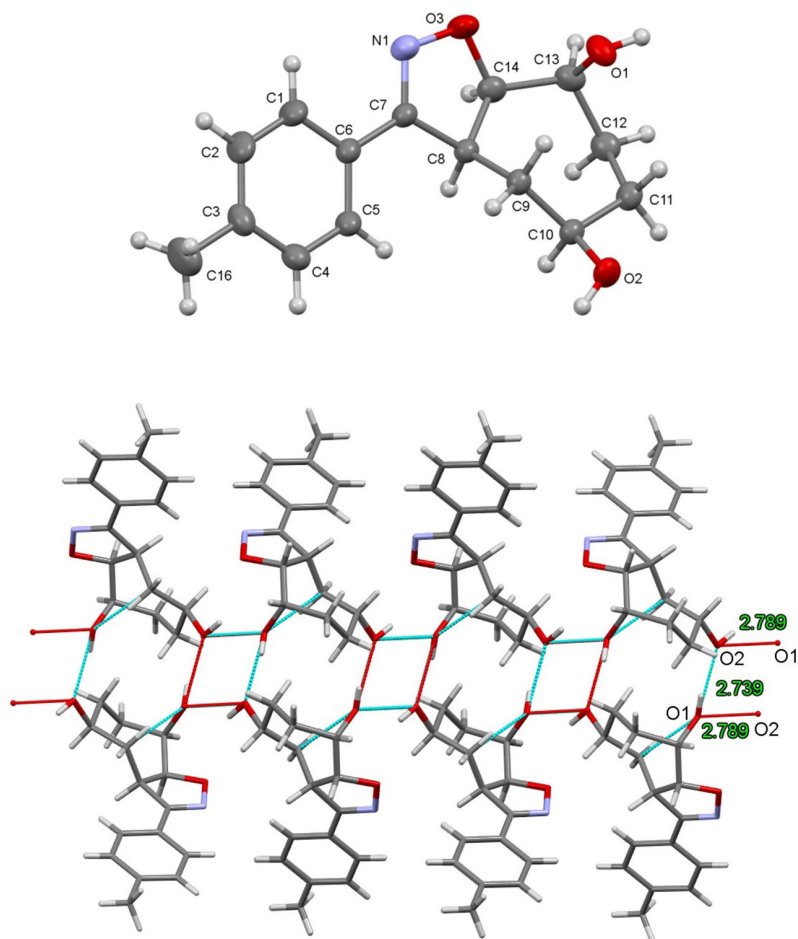


Figure 3. (Top) Molecular structure of **10**. Thermal ellipsoids are drawn at the 40% probability level. (Bottom) Consecutive tetramer chain structure with *H*-bonding geometry.

Furthermore, the reaction of compound **8** with singlet oxygen was performed (Scheme 2). The formation and configuration of endoperoxide **12** formed in this reaction should be very similar to those of endoperoxide **9** because it was also obtained in high yield in its reaction alone. It was accepted that the configuration of **12** was the same as that of **9**.

2.2. DFT calculations

As mentioned above, the formation of a single product in the Diels–Alder reactions of compounds **7** and **8** with dienophiles indicated that there was facial selectivity in them during these reactions. We also focused on testing this selectivity with a theoretical study and examined the mechanism in detail. In our previous research, we used quantum chemical calculations including DFT in the M06-2X method to examine the structural properties of compounds and shed light on the formation mechanism of reactions and obtained quite consistent results [18–20]. The fact that the method used in these studies yielded good results prompted us to use the same method in the quantum chemical calculations in the present study.

2.2.1. Computational details

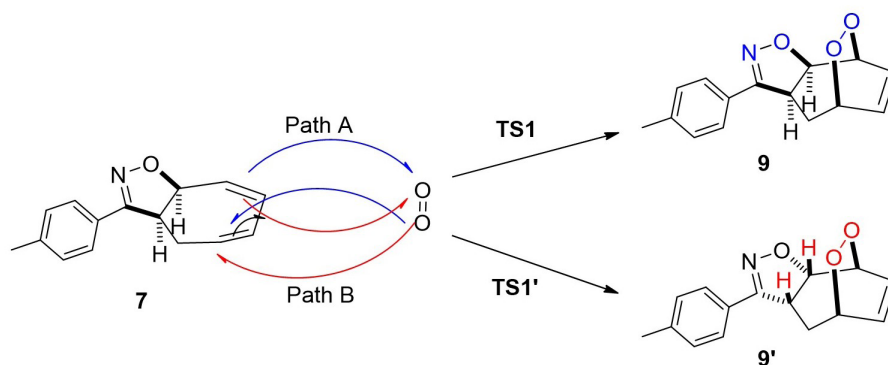
The DFT studies were carried out with the software package Gaussian 09 [21]. The visualizations of the geometric optimizations for all calculations were generated with the program CYLview v1.0.561 BETA [22] and the software GaussView 5.0 [23]. All calculations were performed using DFT with the M06-2X method at the 6-311+G(d,p) level in DCM, and the default polarizable continuum model (PCM) method was used [24,25]. In the present study, we examined the reaction mechanism by optimizing the product (endoperoxide) and the reactant obtained from the intrinsic reaction coordinate (IRC) calculation of the transition state (TS).

2.2.2. Mechanistic calculations

There are two possible pathways for the [4+2] cycloaddition mechanism of $^1\text{O}_2$ to 3-(p-tolyl)-3a,8a-dihydro-4H-cyclohepta[d]isoxazole (7), as shown in Scheme 3. We observed that the endoperoxides (9 and 9') were formed when the products from IRC calculations of the TSs were optimized. In both TSs, the endoperoxide formation reaction occurred in an asynchronous concerted manner by the electrophilic attack of O_2 on C1 and C4 on O1 with singlet oxygen approaching compound 7 from the same (path B) or opposite (path A) direction as H1 and H2.

The first transition state (TS1) corresponds to the electrophilic attack of the singlet oxygen molecule ($^1\text{O}_2$) on the carbon atom (C1) in the less sterically face of diene 7 from the opposite direction as H1 and H2. This transition state is shown as path A in Scheme 3 and Figure 4. In the case of path B, the alternative transition state (TS1') corresponds to the electrophilic attack of O_2 on the C1 atom from the same direction as H1 and H2. The optimized geometries of the transition structures for paths A and B are shown in Figure 4.

The relative Gibbs free energies of both mechanisms are presented in Table. While the TS1' energy barrier of path B (8.3 kcal/mol) is lower than the TS1 energy barrier of path A (9.1 kcal/mol), the relative energy value of the reactant complex



Scheme 3. Paths A and B of the proposed mechanism for the endoperoxides.

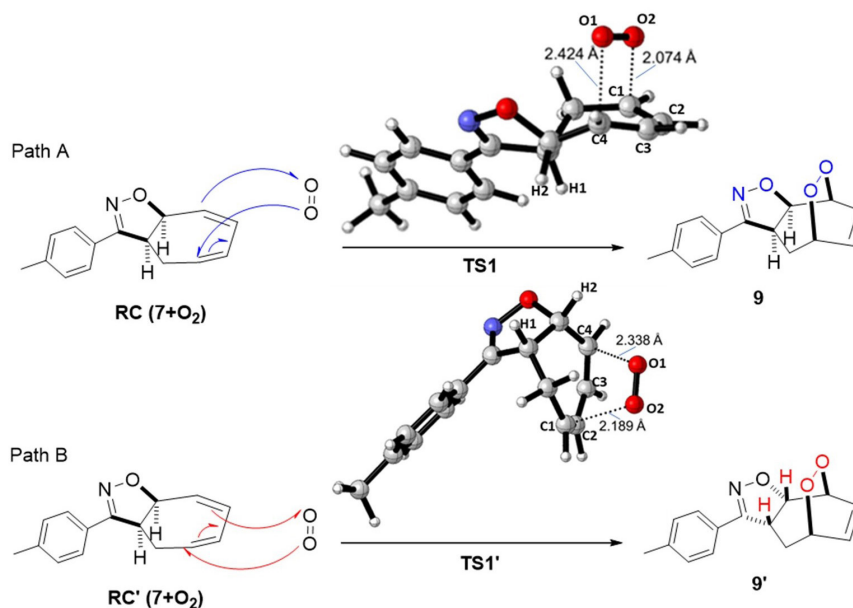


Figure 4. Possible paths A and B for the formation of the transition states TS1 and TS1' for 9 and 9'. Optimized transition structures at PCM/M06-2X/6-311+G(d,p)//M06-2X/6-311+G(d,p) level in DCM.

Table. Gibbs free energies and relative ΔG energies (kcal/mol) of the reactant complexes, transition states, and products for both mechanisms with M06-2X/6-311+G(d,p) level in DCM.

Compound	M06-2X/6-311+G(d,p)	
	Gibbs free energies (au)	ΔG (kcal/mol)
RC (7+ $^1\text{O}_2$)	-860.442697	0.0
RC' (7+ $^1\text{O}_2$)	-860.438132	2.9
TS1	-860.428228	9.1
TS1'	-860.429531	8.3
9	-860.528665	53.9
9'	-860.528323	53.7

(RC') for path B is higher by 2.9 kcal/mol than the energy of the reactant complex (RC) for path A. This result shows that RC is more stable than RC'. Considering the stability of the products obtained from both pathways, it was calculated that the relative Gibbs free energy of product 9 (product compound, PC) was lower by 0.2 kcal/mol than that of product 9' (PC'). According to these results, since the relative energy values of the reactant complex (RC) and product (PC) of path A are lower than those of path B (RC' and PC'), the product to be formed is expected to be obtained from path A. For paths A and B, potential energy profiles in DCM are depicted in Figure 5. The TS1' energy barrier of path B is lower by 0.8 kcal/mol than the TS1 energy value of path A. However, this value represents a very small energy difference for the transition state during the formation of the product. Here the most important driving force in the formation of the product is the relative energy values of the initially formed reactant complex.

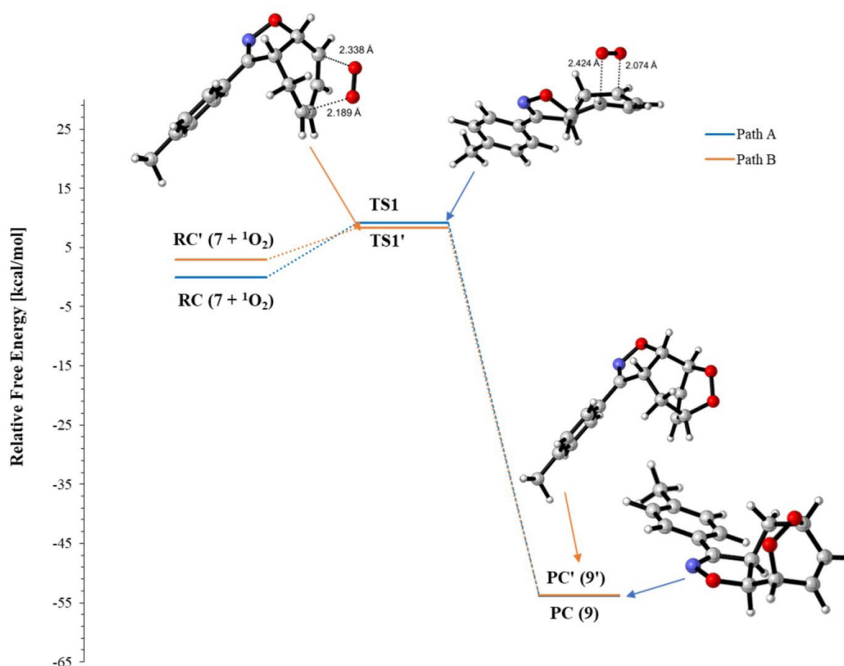


Figure 5. Relative Gibbs free energies (kcal/mol) for the possible paths A and B related to the formation of endoperoxide 9 at PCM/M06-2X/6-311+G(d,p)//M06-2X/6-311+G(d,p) level in DCM.

3. Conclusion

As seen in Scheme 1, two new isoxazole derivatives (**7** and **8**) were synthesized from the reactions of CHT with oximes **4** and **5**. It was observed that the endoperoxides **9** and **12** obtained during their reactions were formed as single products in high yields by the Diels–Alder reaction. Compound **7** was also reacted with PTAD and the adduct **11** was obtained quantitatively from this reaction. Diol **10** was obtained from the reaction of endoperoxide **9** with catalytic hydrogenation. To determine the configurations of endoperoxides (**9** and **12**) and interpret the formation of adducts, X-ray diffraction analyses of compounds **10** and **12** were performed, respectively. Furthermore, the analyses indicated that the observation of facial selectivity in Diels–Alder reactions is the result of the approach of the dienophiles ($^1\text{O}_2$ and PTAD) to the diene moieties of **9** and **10** from only one side. Facial selectivity in the adducts was also investigated theoretically, taking into account the formation of endoperoxide **9**. After the structure of compound **9** was elucidated by X-ray analysis, it was examined by the M06-2X/6-311+G(d,p) level method in DCM to understand the formation mechanism of the product. Our computational studies supported the experimental findings showing that benzoxazole products are formed in this reaction. This research will make significant contributions to the study of elucidating the structure of the products that will be formed during the photooxygenation of isoxazole derivatives in which the cyclic structures are adjacent.

4. Experimental

4.1. General

The chemicals (including solvents) used in the experiments were prepared by known methods. Oximes were synthesized as reported previously [11,13]. The data of the synthesized compounds such as NMR (400 MHz Varian and Bruker), TLC (including preparative TLC), and HRMS [LC–MS–TOF electrospray ionization (1200/6210, Agilent)] were obtained as explained previously [7,11,12,26–28]. All NMR and HRMS spectra are given in Supplementary Material.

4.2. Synthesis of 3-(*p*-tolyl)-3a,8a-dihydro-4*H*-cyclohepta[d]isoxazole (**7**)

A stirring solution of compound **4** (2.6 g, 1.0 equiv.) and **6** (5.0 equiv.) in CH_2Cl_2 (30 mL) was cooled in the ice bath and then a solution of NEt_3 (2.98 g, 2.0 equiv.) in CH_2Cl_2 (10 mL) was added dropwise to this solution. After the mixture was stirred for 2 days without further bath cooling, the reaction mixture was monitored by TLC and the reaction was completed. Water (15 mL) was added to the mixture and then the pH of the mixture was adjusted to 6–7 with dilute HCl solution. The mixture was extracted with CH_2Cl_2 (2×15 mL) and after the organic phases were combined, the resulting solution was dried over Na_2SO_4 , and the solvent was removed under low pressure. Compound **7** (3.13 g, 90%) was obtained from the purification of crude product on silica gel (45 g) column chromatography (CC) by EtOAc/petroleum ether (5/95) elution. Mp: 83–85 °C; $^1\text{H-NMR}$ (400 MHz, CDCl_3): 7.63 (d, $J = 8.4$ Hz, A part of AB system, 2H), 7.24 (d, $J = 8.4$ Hz, B part of AB system, 2H), 6.32 (dd, $J = 11.6, 3.2$ Hz, A part of AB system, 1H), 6.22–6.05 (m, 3H), 4.95 (dd, $J = 8.5, 2.8$ Hz, OCH, 1H), 3.40 (ddd, $J = 9.6, 8.5, 2.2$ Hz, CCH, 1H), 2.39 (s, CH_3 , 3H), 2.34–2.25 (m, 1H), 2.20–2.09 (m, 1H); $^{13}\text{C-NMR}$ (100 MHz, CDCl_3): 160.94 (CN), 140.43 (C), 133.26 (CH), 129.60 (2 CH), 128.64 (CH), 127.79 (CH), 126.97 (2 CH), 126.81 (CH), 125.84 (C), 83.08 (OCH), 50.82 (CH), 27.01 (CH_2), 21.63 (CH_3); R_f : 0.51 EtOAc/hexane (1/19); HRMS: (APCI – TOF) (m/z) calcd for $[\text{C}_{15}\text{H}_{15}\text{NO} + \text{H}]^+$: 226.12319; found: 226.12249.

4.3. Synthesis of 3-(4-methoxyphenyl)-3a,8a-dihydro-4*H*-cyclohepta[d]isoxazole (**8**)

A stirring mixture of oxime **5** (5.0 g, 33.1 mmol, 1.0 equiv.), CHT (15.2 g, 5.0 equiv.), and CH_2Cl_2 (100 mL) was cooled with ice. Next, cold aqueous NaOCl (sodium hypochlorite) solution (5.25%, 45 mL, 1.072 g/mL) solution was added to the mixture, and then the mixture was stirred for 3 days without further bath cooling. After the organic phase of the mixture was separated and the aqueous phase was extracted with CH_2Cl_2 (2×30 mL), the combined organic phases were dried over Na_2SO_4 and the solvent was removed by rotary evaporator. The reaction mixture was subjected to CC on silica gel (55 g) and eluted using EtOAc/petroleum ether (by changing from 15/85 to 30/70). Product **8** (6.1 g, 76%) was obtained almost pure, and **8** was also obtained from this product pure using EtOAc/petroleum ether (30/70) by preparative TLC. Mp: 105–107 °C; $^1\text{H-NMR}$ (400 MHz, CDCl_3): 7.68 (d, $J = 9.0$ Hz, A part of AB system, 2H), 6.94 (d, $J = 9.0$ Hz, B part of AB system, 2H), 6.31 (dd, $J = 11.6, 3.2$ Hz, A part of AB system, 1H), 6.22–6.02 (m, 3H), 4.92 (dd, $J = 8.4, 3.2$ Hz, CHO, 1H), 3.85 (s, OMe, 3H), 3.37 (ddd, $J = 17.2, 8.4, 2.0$ Hz, CCH, 1H), 2.28 (bdd, $J = 8.4, 3.2$ Hz, A part of AB system, CH_2 , 1H), 2.19–2.08 (m, CH_2 , 1H); $^{13}\text{C-NMR}$ (100 MHz, CDCl_3): 161.30 (C), 160.86 (C), 133.49 (CH), 128.79 (CH), 128.76, 127.98 (2 CH), 126.99 (CH), 121.66 (CH), 114.56 (2 CH), 83.12 (OCH), 55.67, 51.25, 27.29 (CH_2); R_f : 0.54 EtOAc/hexane (1/5); HRMS (APCI – TOF) (m/z) calcd for $[\text{C}_{15}\text{H}_{15}\text{NO}_2 + \text{H}]^+$: 242.11810; found: 242.11699.

4.4. Photooxygenation of compound **7**

A solution of compound **7** (650 mg) and catalytic tetraphenylporphyrin (TPP) in CH_2Cl_2 (90 mL) was placed in a flask continuously cooled by tap water on the outside. This solution was irradiated with a projector lamp (150 W) while a slow

stream of dry O₂ was passed through it continuously. The reaction was continuously checked by TLC, and after 6 days, the solvent was removed at room temperature in a rotary evaporator. The resulting endoperoxide **9** (713 mg, 96%) was crystallized by spontaneously removing the solvent from its concentrated solution in CH₂Cl₂ at RT. (3aS*,5S*,8S*,8aR*)-3-(*p*-tolyl)-3a,5,8,8a-tetrahydro-4*H*-5,8-epidioxycyclohepta[*d*]isoxazole (**9**): Mp: 157–159 °C; ¹H-NMR (400 MHz, CCl₄): 7.53 (d, *J* = 7.8 Hz, A part of AB system, 2H), 7.21 (d, *J* = 7.8 Hz, B part of AB system, 2H), 6.74–6.67 (m, 1H), 6.58–6.52 (m, 1H), 5.15 (d, *J* = 5.9 OCH, 1H), 4.82 (dd, *J* = 9.6, 5.9 OCH, 1H), 4.76 (t, *J* = 5.9 OCH, 1H), 3.68–3.60 (m, CCH, 1H), 2.59–2.50 (m, CH₂, 1H), 2.34 (s, CH₃, 3H), 2.43–2.33 (m, CH₂, 1H); ¹³C-NMR (100 MHz, CDCl₃): 160.72 (CN), 140.57 (C), 139.90 (CH), 129.61 (2 CH), 127.10 (2 CH), 125.84 (C), 84.93 (OCH), 75.96 (OCH), 74.15 (OCH), 43.75 (CH), 34.09 (CH₂), 21.44 (CH₃); R_f: 0.41 EtOAc/hexane (2/3); HRMS: *m/z* (M+ 3H) calcd. For C₁₅H₁₈NO₃: 260.12867; Found: 260.12882.

4.5. Catalytic hydrogenation of endoperoxide **9**

After compound **9** (300 mg, 1.17 mmol), Pd/C catalyst (6 mg), and EtOAc (30 mL) were placed in a flask (100 mL, two-necked) fitted with a spin bar at RT, the air in the flask was replaced 3 times by hydrogen gas (about 1 atm in the balloon attached to the flask). Subsequently, the reaction was started, checked from time to time by TLC, and terminated after 5 days. The reaction mixture was filtered through filter paper to remove the catalyst and EtOAc was removed by rotary evaporator at RT. Diol **10** (115 mg, 38%) was obtained from the purification of residue on silica gel column chromatography (25 g) with EtOAc/petroleum ether (2/3) and crystallized in the mixture of CHCl₃/hexane. (3aS*,5R*,8S*,8aR*)-3-(*p*-tolyl)-3a,5,6,7,8,8a-hexahydro-4*H*-cyclohepta[*d*]isoxazole-5,8-diol (**10**): Mp: 198–200 °C; ¹H NMR [400 MHz, (CD)₃CO]: 7.54 (d, *J* = 8.0 Hz, A part of AB system, 2H), 7.25 (d, *J* = 8.0 Hz, B part of AB system, 2H), 4.57 (dd, *J* = 11.6, 3.6 Hz, A part of AB system, 1H), 4.29–4.23 (m, 1H), 4.00–3.91 (m, 2H), 3.68–3.3.60 (m, 5H), 2.87 (3, 3H), 2.23–2.12 (m, 1H), 2.06–1.92 (m, 5H), 1.83–1.73 (m, 1H), 1.59–1.50 (m, 1H); ¹³C NMR [400 MHz, (CD)₃CO]: 159.49 (NC) 139.42 (C), 129.47 (2 CH), 127.27 (2 CH), 126.97 (C), 86.64 (OCH), 72.29 (OCH), 67.65 (OCH), 37.16, 32, 32.09, 26.31, 20.64; R_f: 0.26 EtOAc/hexane (1/3); HRMS (APCI – TOF) (*m/z*) calcd for [(C₁₅H₁₉NO₃) + H]⁺: 262.14432; found: 262.14353.

4.6. Cycloaddition reaction of compound **7** with PTAD

PTAD (80 mg, 0.46 mmol, 1.0 equiv.) was added to a solution of the compound **7** (103 mg) in CH₂Cl₂ (15 mL) at RT. The mixture was stirred for 1 day and it was observed that its red color changed to pale yellow. Adduct **11** (183 mg, quantitative) was obtained and crystallized from EtOAc. (3aS*,5S*,11S*,11aR*)-8-phenyl-3-(*p*-tolyl)-3a,4,11,11a-tetrahydro-5*H*,7*H*-5,11-ethenoisoxazolo[5,4-*d*][1,2,4]triazolo[1,2-*a*][1,2]diazepine-7,9(8*H*)-dione (**11**). Mp: 193–195 °C; ¹H-NMR (400 MHz, CDCl₃): 7.51–7.35 (m, 7H), 7.24 (d, *J* = 8.0 Hz, B part of AB system, 2H), 6.49 (dd, *J* = 8.8, 6.6 Hz, A part of AB system, 1H), 6.25 (ddd, *J* = 8.8, 6.6, 0.5 Hz, B part of AB system, 1H), 5.21–5.18 (m, NCH, 1H), 5.03 (dd, *J* = 9.8, 4.6 OCH, 1H), 4.94–4.91 (m, NCH, 1H), 4.25 (dt, *J* = 9.8, 4.0 CCH, 1H), 2.47 (ddd, *J* = 14.7, 9.2, 3.6 Hz, A part of AB system, CH₂, 1H), 2.40 (s, CH₃, 3H), 2.18 (dt, *J* = 14.7, 4.3 Hz, B part of AB system, CH₂, 1H); ¹³C-NMR (100 MHz, CCl₄): 161.63 (CN), 151.78 (CO), 151.43 (CO), 140.85 (C), 131.49 (C), 129.99 (CH), 129.81 (2 CH), 129.20 (2 CH), 129.07 (CH), 128.34 (CH), 127.50 (2 CH), 126.56 (2 CH), 124.84 (C), 81.07 (OCH), 51.48 (NCH), 49.29 (NCH), 45.29 (CH), 27.75 (CH₂), 21.23 (CH₃); R_f: 0.52 EtOAc/hexane (1/1); HRMS (APCI – TOF) (*m/z*) calcd for [(C₂₃H₂₀N₄O₃) + H]⁺: 401.16137; found: 401.16017.

4.7. Photooxygenation of compound **8**

The reaction was carried out like the photooxygenation of compound **7** in 4.4. The reaction was realized according to procedure 1. Compound **8** (180 mg), CH₂Cl₂ (70 mL), and TPP (catalytic) were used in the reaction. The reaction lasted 3 days and its crystallization was carried out like that of endoperoxide **9**. (3aS*,5S*,8S*,8aR*)-3-(4-methoxyphenyl)-3a,5,8,8a-tetrahydro-4*H*-5,8-epidioxycyclohepta[*d*]isoxazole (**12**) (183 mg, 90%) was obtained from the reaction. Mp: 161–163 °C; ¹H-NMR (400 MHz, CDCl₃): ¹H NMR (400 MHz, (CDCl₃): 7.57 (d, *J* = 9.2 Hz, A part of AB system, 2H), 6.91 (d, *J* = 9.2 Hz, B part of AB system, 2H), 6.69 (dd, *J* = 9.1, 7.0 Hz, A part of AB system, 1H), 6.54 (ddd, *J* = 9.1, 7.0, 2.0 Hz, B part of AB system, 1H), 5.14 (dm, *J* = 6.4 Hz, NOCH, 1H), 4.82–4.73 (m, OCH, 2H), 3.82 (OMe), 3.61 (dt, *J* = 10.0, 8.4 Hz CCHC, 1H), 2.55 (ddd, *J* = 15.2, 8.4, 5.8 Hz, CH₂, 1H), 2.45 (ddd, *J* = 15.2, 10.4, 1.6 Hz, CH₂, 1H); ¹³C-NMR (100 MHz, CDCl₃): 161.38 (CN or CO), 160.65 (CN or CO), 134.15 (CH), 128.87 (2 CH), 127.35 (CH), 121.31 (C), 114.54 (2 CH), 85.09 (OCH), 86.19 (OCH), 85.09 (OCH), 74.27 (OCH), 55.62 (OCH₃), 44.04 (CH), 34.35 (CH₂); R_f: 0.24 EtOAc/hexane (2/3); HRMS (APCI – TOF) (*m/z*) calcd for [C₁₅H₁₅NO₂ + H]⁺: 274.10793; found: 274.10642.

4.8. Crystal structure determination

For the crystal structure determination, single crystals of the molecules of **9** and **10** were used for data collection on a four-circle Rigaku R-AXIS RAPID-S diffractometer (equipped with a two-dimensional area IP detector). Graphite-monochromated Mo-Kα radiation (*l* = 0.71073 Å) and oscillation scans with *Dw* = 5° for one image were used for data

collection. The lattice parameters were determined by the least-squares methods on the basis of all reflections with $F^2 > 2s(F^2)$. Integration of the intensities, correction for Lorentz and polarization effects, and cell refinement were performed using the software CrystalClear (Rigaku/MSC Inc., 2005) [29]. The structures were solved by direct methods using SHELXS-2013 [30], which allowed location of most of the heaviest atoms, with the remaining nonhydrogen atoms being located from difference Fourier maps calculated from successive full-matrix least squares refinement cycles on F^2 using SHELXL-2013 [30]. All nonhydrogen atoms were refined using anisotropic displacement parameters. The hydrogen atoms were assigned with common isotropic displacement factors and included in the final refinement using geometrical restrains. The final difference Fourier maps showed no peaks of chemical significance. *Crystal data for 9*: $C_{15}H_{15}O_3N$, crystal system, space group: orthorhombic, Iba2; (no: 45); unit cell dimensions: $a = 13.3717(5)$, $b = 26.251(2)$, $c = 8.3998(3)$ Å, $\alpha = 90$, $\beta = 90$, $\gamma = 90^\circ$; volume; $2948.5(2)$ Å³, $Z = 8$; calculated density: 1.159 g/cm³; absorption coefficient: 0.663 mm⁻¹; $F(000)$: 1088; θ -range for data collection 3.3 – 74.9° ; refinement method: full matrix least-square on F^2 ; data/parameters: 2627/174; goodness-of-fit on F^2 : 1.108; final R-indices [$I > 2s(I)$]: $R_1 = 0.086$, $wR_2 = 0.224$; largest diff. peak and hole: 0.360 and -0.407 e Å⁻³. *Crystal data for 10*: $C_{15}H_{19}NO_3$, crystal system, space group: monoclinic, $P2_1/c$; (no: 14); unit cell dimensions: $a = 17.522(4)$, $b = 6.6629(3)$, $c = 11.695(2)$ Å, $\alpha = 90$, $\beta = 97.951(8)$, $\gamma = 90^\circ$; volume; $1352.2(5)$ Å³, $Z=4$; calculated density: 1.284 g/cm³; absorption coefficient: 0.724 mm⁻¹; $F(000)$: 560; θ -range for data collection 2.5 – 79.4° ; refinement method: full matrix least-square on F^2 ; data/parameters: 2387/176; goodness-of-fit on F^2 : 1.085; final R-indices [$I > 2s(I)$]: $R_1 = 0.045$, $wR_2 = 0.126$; largest diff. peak and hole: 0.210 and -0.161 e Å⁻³.

CCDC-2316861 (9) and 2320571 (10) numbers contain the supplementary crystallographic data. These data are provided free of charge via the joint CCDC/FIZ Karlsruhe deposition service: www.ccdc.cam.ac.uk/structures

Acknowledgments

This study was carried out at Atatürk University, Faculty of Science, Department of Chemistry. The authors thank the TÜBİTAK-ULAKBİM, High Performance and Grid Computing Center (TRUBA resources) for computer time. We also thank the institution for their support.

References

- [1] Balci M. Bicyclic Endoperoxides and synthetic applications. *Chemical Reviews* 1981; 81 (1): 91–108. <https://doi.org/10.1021/cr00041a005>
- [2] Akbulut N, Menzek A, Balci M. Thermolysis and CoTPP-catalyzed rearrangement of endoperoxides derived from 2,3-dihydro-1(2H) azulenone: a new endoperoxide-endoperoxide rearrangement. *Tetrahedron Letters* 1987; 28 (15): 1689–1692. [https://doi.org/10.1016/S0040-4039\(00\)95395-4](https://doi.org/10.1016/S0040-4039(00)95395-4)
- [3] Johnson CR, Golebiowski A, McGill TK, Steensma DH. Enantioselective synthesis of 6-cycloheptene-1,3,5-triol derivatives by enzymatic asymmetrization. *Tetrahedron Letters* 1991; 32 (23): 2597–2600. [https://doi.org/10.1016/S0040-4039\(00\)78794-6](https://doi.org/10.1016/S0040-4039(00)78794-6)
- [4] Menzek A, Şengül ME, Çetinkaya Y, Ceylan S. Photooxygenation of 5- and 6-chloro-1,3-cycloheptadienes and reactions of their endoperoxides with base: effects of the chloro substituent on the reactions. *Journal of Chemical Research* 2005; (4): 209–214. <https://doi.org/10.3184/0308234054213492>
- [5] Paquette LA, Shen CC. Synthesis, static structure, and kinetic stability of a syn-sesquinorbornatriene. *Journal of the American Chemical Society* 1990; 112 (3): 1159–1164. <https://doi.org/10.1021/ja00159a041>
- [6] Menzek A, Kelebekli L, Altundaş A, Şahin E, Polat F. Cycloaddition reaction of 1,4-dihydronaphthalene 1,4-epoxide with cyclooctatetraene: cope rearrangement in an adduct. *Helvetica Chimica Acta* 2008; 91 (12): 2367–2378. <https://doi.org/10.1002/hlca.200890257>
- [7] Adiloğlu Y, Şahin E, Tutar A, Menzek A. Cycloaddition reactions of benzonorbornadiene and homonorbornadiene: new isoxazoline and pyridazine derivatives. *Journal of Heterocyclic Chemistry* 2018; 55 (8): 1917–1927. <https://doi.org/10.1002/jhet.3229>
- [8] Menzek A, Altundaş A, Çoruh U, Akbulut N, Vázquez López EM et al. Cycloaddition reactions of 1,4-dihydronaphthalene-1,4-epoxide with cyclohexadiene and 7-(methoxycarbonyl)cycloheptatriene: selectivity in additions. *European Journal of Organic Chemistry* 2004; (5): 1143–1148. <https://doi.org/10.1002/ejoc.200300569>
- [9] Gandolfi R, Tonoletti G, Rastelli A, Bagatti M. 2,3-Dioxabicyclo[2.2.2]oct-5-ene: a pyramidalized olefin whose facial selectivity does not parallel its pyramidalization. *Journal of Organic Chemistry* 1993; 58 (22): 6038–6048. <https://doi.org/10.1021/jo00074a034>
- [10] Gamba A, Gandolfi R, Gruenanger P. ChemInform abstract: reactions of nitrile oxides and nitrile imides with cycloheptatriene and (cycloheptatriene)tricarbonyliron. *ChemInform* 1993; 24 (37): 209–214. <https://doi.org/10.1002/chin.199337098>

- [11] Schwarz L, Girreser U, Clement B. Synthesis and characterization of para-substituted N,N'- dihydroxybenzamidines and their derivatives as model compounds for a class of prodrugs. *European Journal of Organic Chemistry* 2014; 2014 (9): 1961–1975. <https://doi.org/10.1002/ejoc.201301622>
- [12] Yavari MA, Adiloglu Y, Saglamtas R, Tutar A, Gulcin I et al. Synthesis and some enzyme inhibition effects of isoxazoline and pyrazoline derivatives including benzonorbornene unit. *Journal of Biochemical and Molecular Toxicology* 2022; 36 (2): e22952. <https://doi.org/10.1002/jbt.22952>
- [13] Yavari MA, Taslimi P, Bayrak C, Taskin-Tok T, Menzek A. 1,3-dipolar cycloaddition reactions of the compound obtaining from cyclopentadiene-PTAD and biological activities of adducts formed selectively. *Journal of Heterocyclic Chemistry* 2022; 59 (5): 864–878. <https://doi.org/10.1002/jhet.4426>
- [14] Sengül ME, Menzek A, Sahin E, Arik M, Saracoglu N. Synthesis of cyclopropane-annulated conduritols derivatives: norcaran-2,3,4,5-tetraols. *Tetrahedron* 2008; 64 (30–31): 7289–7294. <https://doi.org/10.1016/j.tet.2008.05.066>
- [15] Şenol H, Bayrak Ç, Menzek A, Şahin E, Karakuş M. Cycloaddition reaction of spiro[2.4]hepta-4,6-dien-1-ylmethanol and PTAD: a new rearrangement. *Tetrahedron* 2016; 72 (20): 2587–2592. <https://doi.org/10.1016/j.tet.2016.03.094>
- [16] Donohoe TJ. *Oxidation and Reduction in Organic Synthesis*. Oxford, UK: Oxford University Press, 2000.
- [17] Artunç T, Menzek A. Synthesis and reactions of di(thiophen-2-yl)alkane diones: cyclocondensation. *Turkish Journal of Chemistry* 2022; 46 (5): 1397–1404. <https://doi.org/10.55730/1300-0527.3446>
- [18] Çetinkaya Y, Maraş A, Göksu S. Insight into the intramolecular interactions of trans-2-azidocycloalk-3-en-1-ols and trans-2-azidocycloalk-3-en-1-yl acetates: a theoretical study. *Tetrahedron* 2021; 92: 132272. <https://doi.org/10.1016/j.tet.2021.132272>
- [19] Demir E, Sari O, Çetinkaya Y, Atmaca U, Erdem SS et al. One-pot synthesis of oxazolidinones and five-membered cyclic carbonates from epoxides and chlorosulfonyl isocyanate: theoretical evidence for an asynchronous concerted pathway. *Beilstein Journal of Organic Chemistry* 2020; 16: 1805–1819. <https://doi.org/10.3762/bjoc.16.148>
- [20] Çetinkaya Y, Artunç T, Menzek A. AlCl₃-catalyzed cascade reactions of 1,2,3-trimethoxybenzene and adipoyl chloride: spectroscopic investigations and density functional theory studies. *ACS Omega* 2022; 7 (43): 38882–38893. <https://doi.org/10.1021/acsomega.2c04612>
- [21] Frisch MJ, Trucks GW, Schlegel HB, Scuseria GE, Robb MA et al. *Gaussian 09, Revision C. 01*, Gaussian Inc.: Wallingford CT. 2010.
- [22] Legault CY. *CYLview, 1.0b*. Université de Sherbrooke, Québec, Canada 2009.
- [23] Dennington R, Keith T, Millam J. *GaussView 5.0*. Semichem Inc., Shawnee Mission, KS 2009.
- [24] Zhao Y, Truhlar DG. The M06 suite of density functionals for main group thermochemistry, thermochemical kinetics, noncovalent interactions, excited states, and transition elements: two new functionals and systematic testing of four M06 functionals and 12 other functionals. *Theoretical Chemistry Accounts* 2008; 119 (5–6): 525. <https://doi.org/10.1007/s00214-007-0401-8>
- [25] Zhao Y, Truhlar DG. Density functionals with broad applicability in chemistry. *Accounts of Chemical Research* 2008; 41 (2): 157–167. <https://doi.org/10.1021/ar700111a>
- [26] Aydin G, Ally K, Aktaş F, Şahin E, Baran A et al. Synthesis and α-glucosidase and α-amylase inhibitory activity evaluation of azido- and aminocyclitols. *European Journal of Organic Chemistry* 2014; 2014 (31): 6903–6917. <https://doi.org/10.1002/ejoc.201402762>
- [27] Menzek A, Balci M. Cycloaddition reactions of substituted cycloheptatrienes with benzyne and quinones: an entry to the substituted benzhomobarrelenes. *Tetrahedron* 1993; 49 (27):6071–6078. [https://doi.org/10.1016/S0040-4020\(01\)87191-X](https://doi.org/10.1016/S0040-4020(01)87191-X)
- [28] Şengül ME, Menzek A, Saraçoğlu N. Synthesis of cycloheptane-1,2,3,4-tetraols as cyclitol mimetics. *Journal of Chemical Research* 2005; (6): 382–384. <https://doi.org/10.3184/0308234054506794>
- [29] Rigaku/MSc, Inc., 9009 new Trails Drive, TheWoodlands, TX 77381.
- [30] Sheldrick GM. *SHELXS-97 and SHELXL-97*, Program for Crystal Structure Solution and Refinement. 1997.

Supplementary Material

Content

Figures S1–S18 ¹H, ¹³C NMR, and HRMS spectra of compounds 7–12. Cartesian coordinates for the optimized structures.

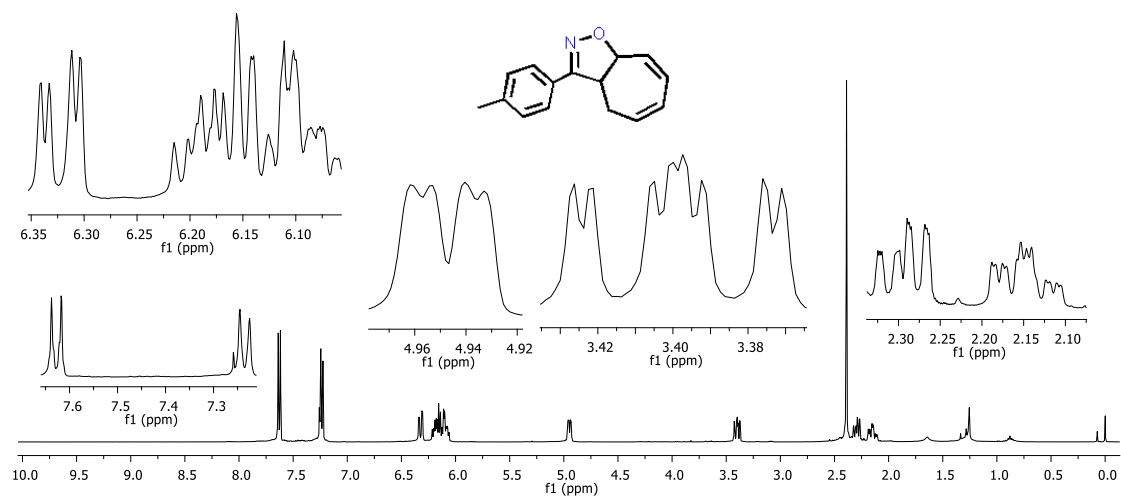


Figure S1. ¹H-NMR spectrum of 7 (400 MHz, CDCl₃).

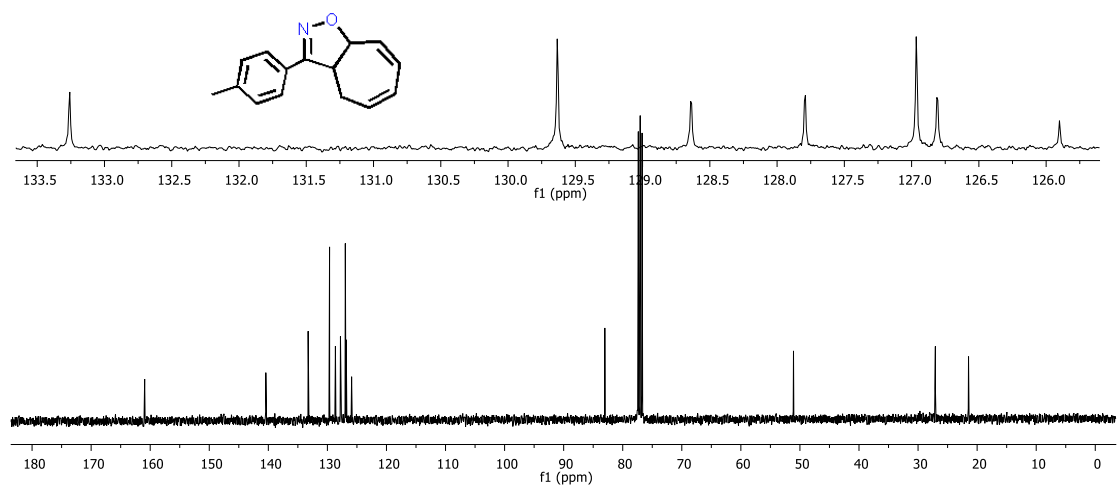


Figure S2. ¹³C-NMR spectrum of 7 (100 MHz, CDCl₃).

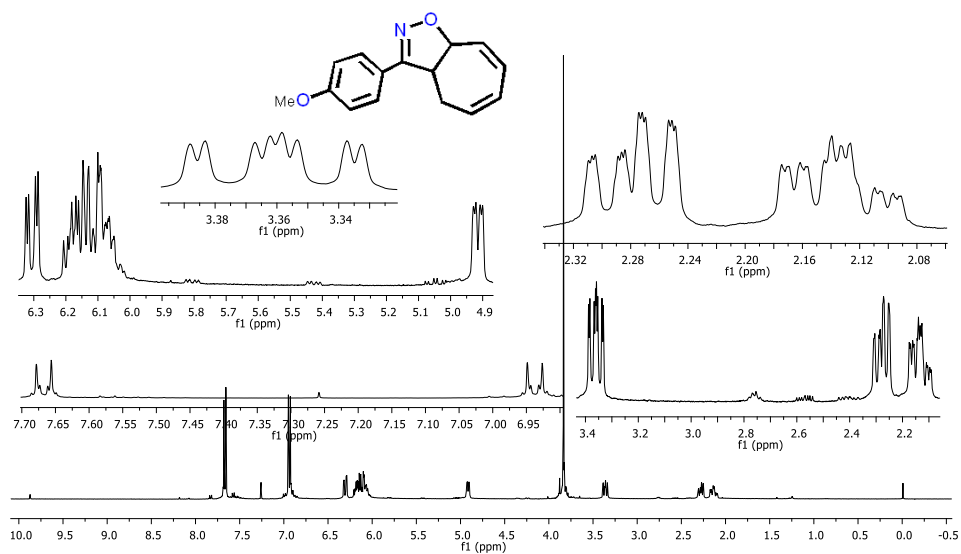


Figure S3. ¹H-NMR spectrum of **8** (400 MHz, CDCl₃).

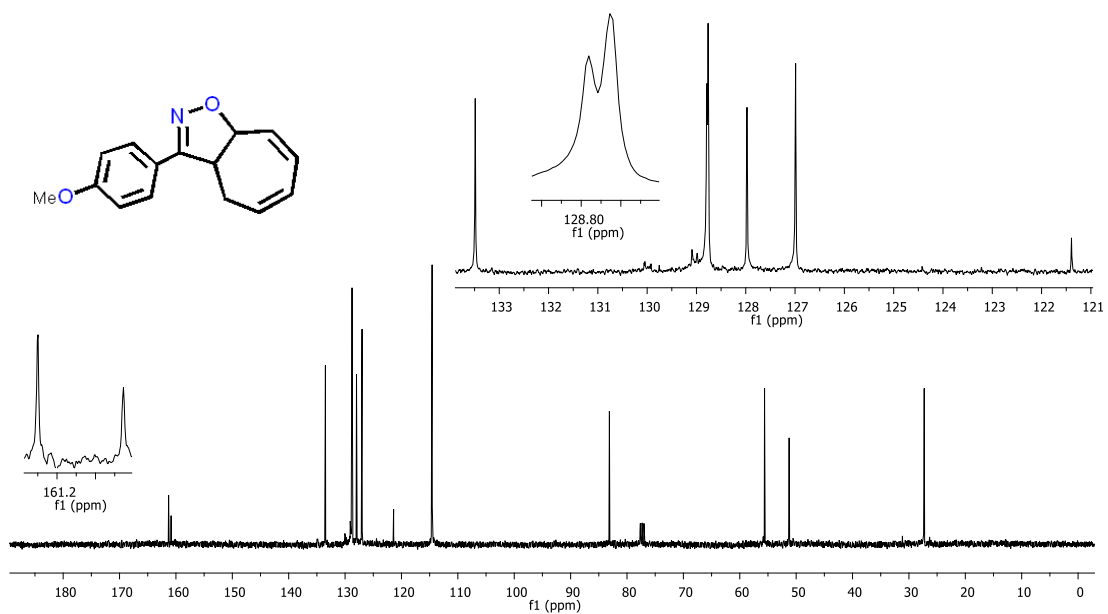


Figure S4. ¹³C-NMR Spectrum of **8** (100 MHz, CDCl₃).

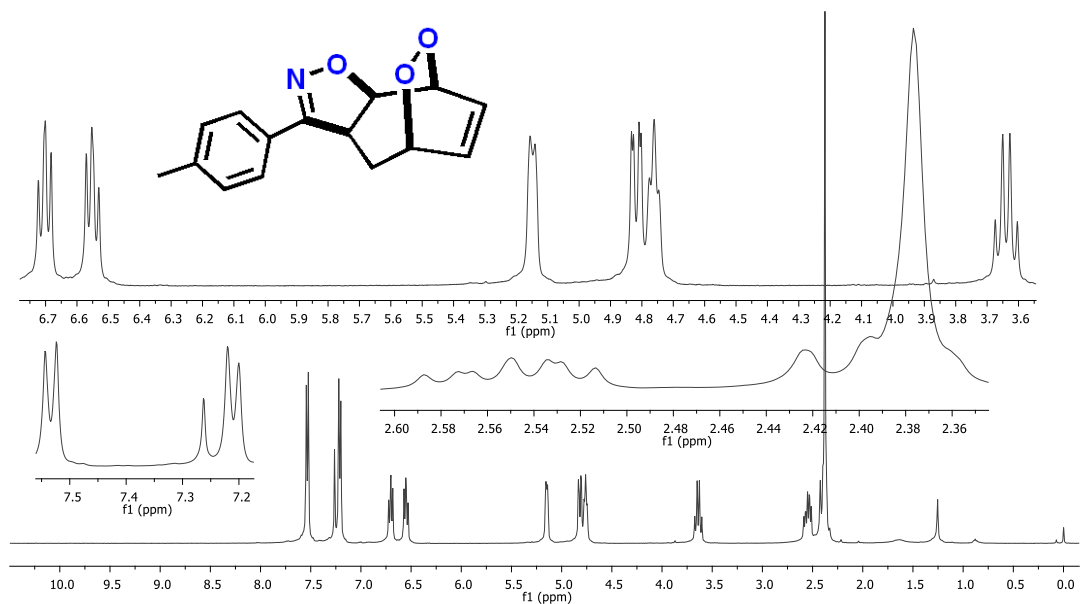


Figure S5. ¹H-NMR spectrum of 9 (400 MHz, CDCl₃).

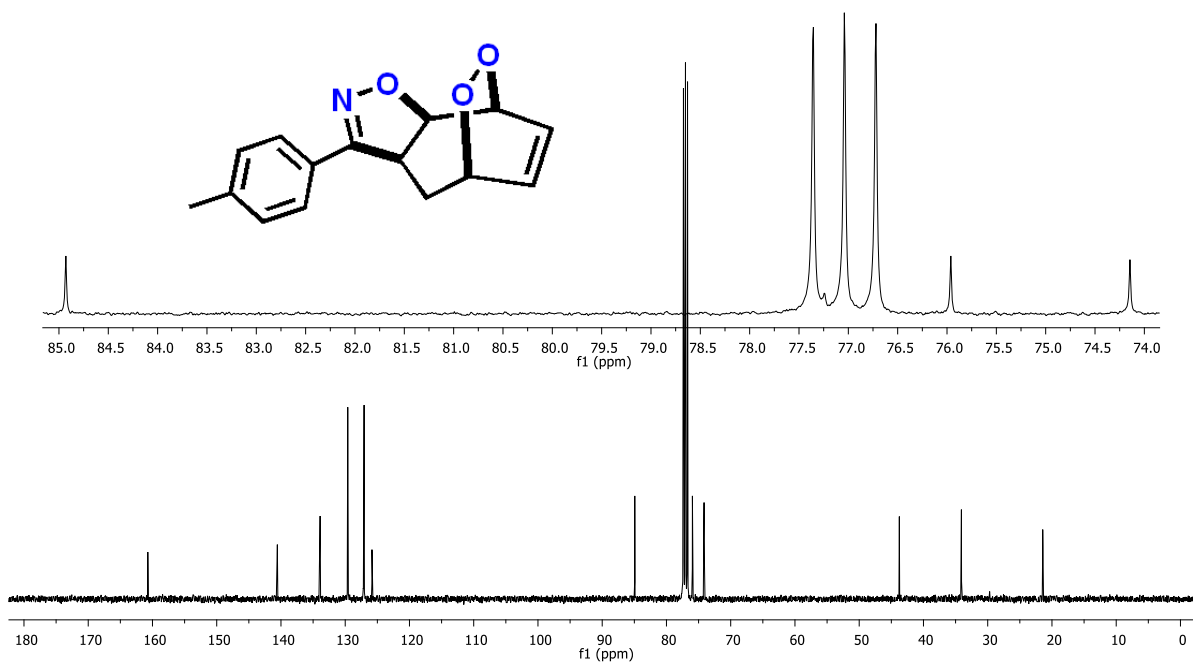


Figure S6. ¹³C-NMR spectrum of 9 (100 MHz, CDCl₃).

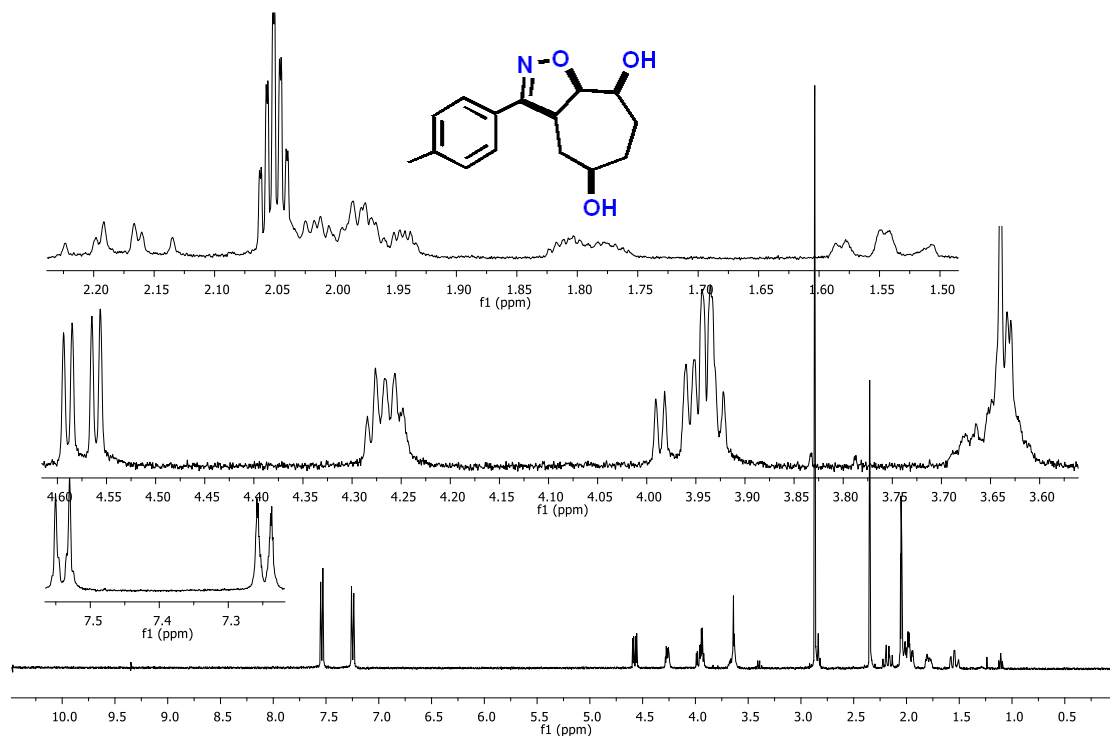


Figure S7. ¹H-NMR spectrum of **10** [400 MHz, (CD)₃CO].

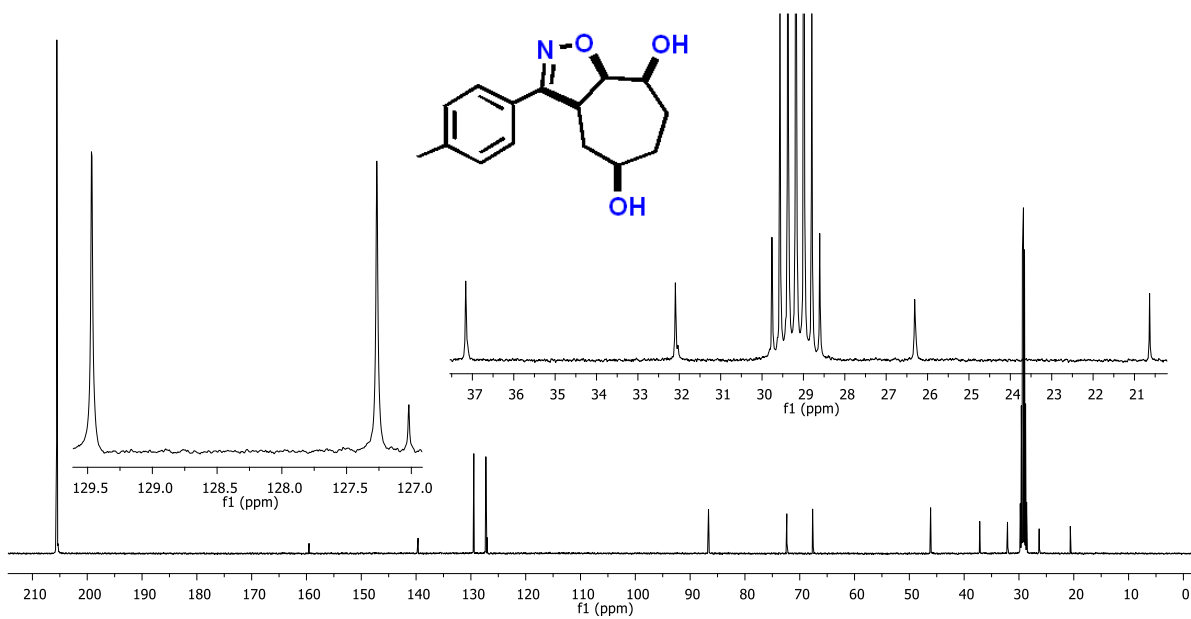


Figure S8. ¹³C-NMR spectrum of **10** [100 MHz, (CD)₃CO].

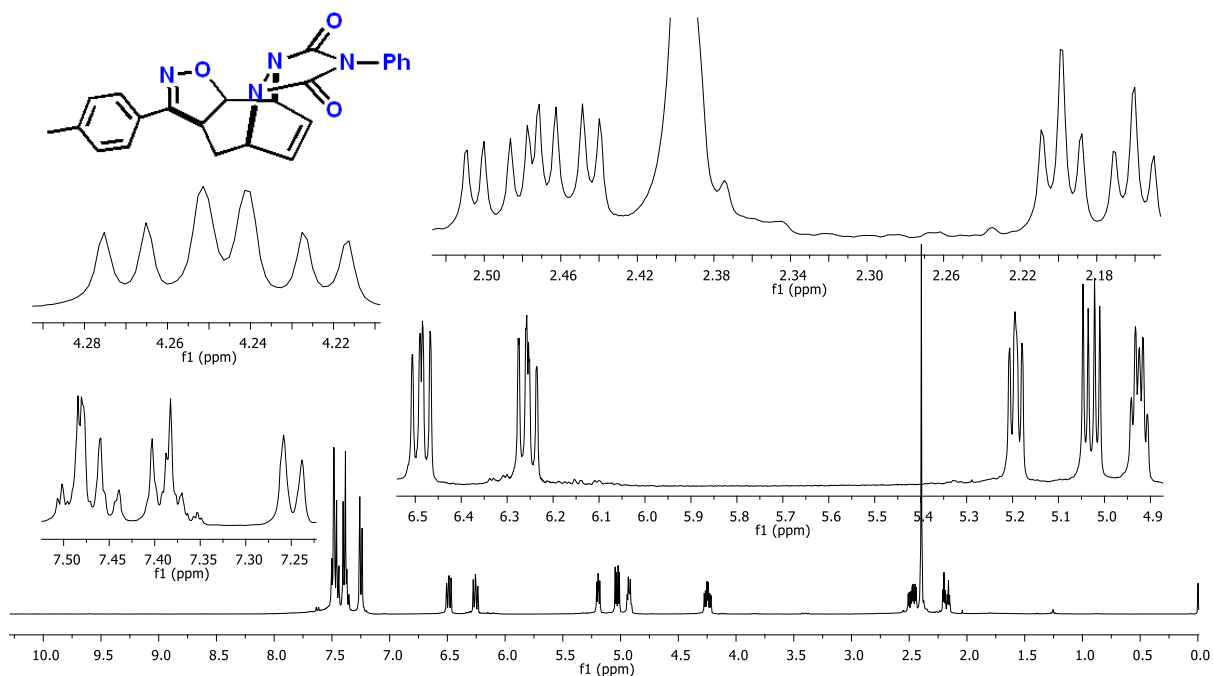


Figure S9. ¹H-NMR spectrum of **11** (400 MHz, CDCl₃).

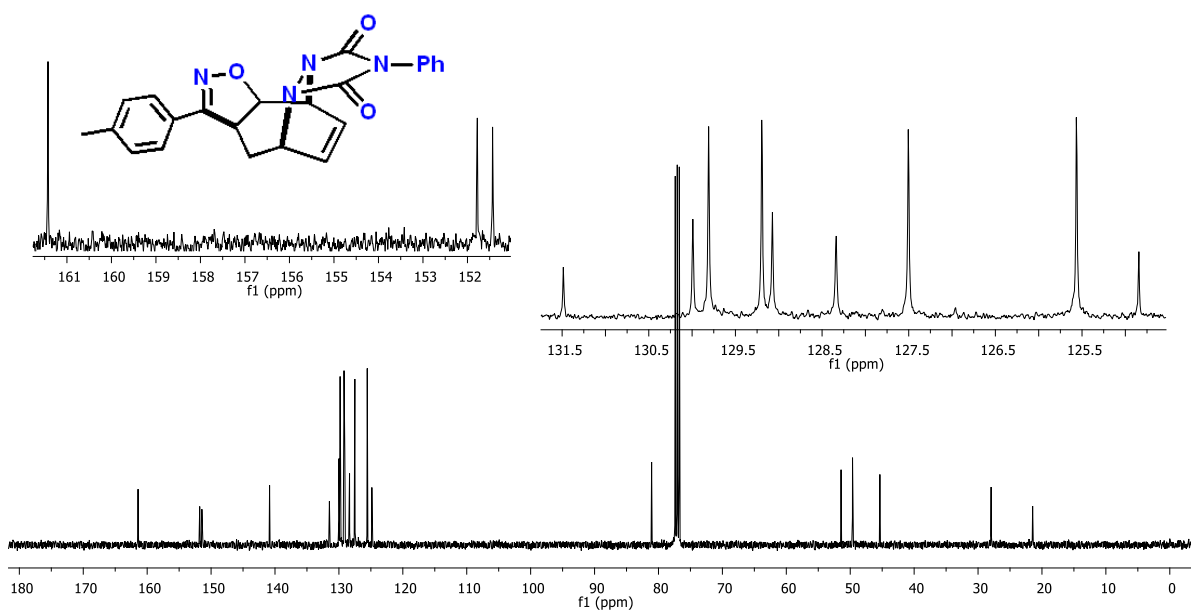
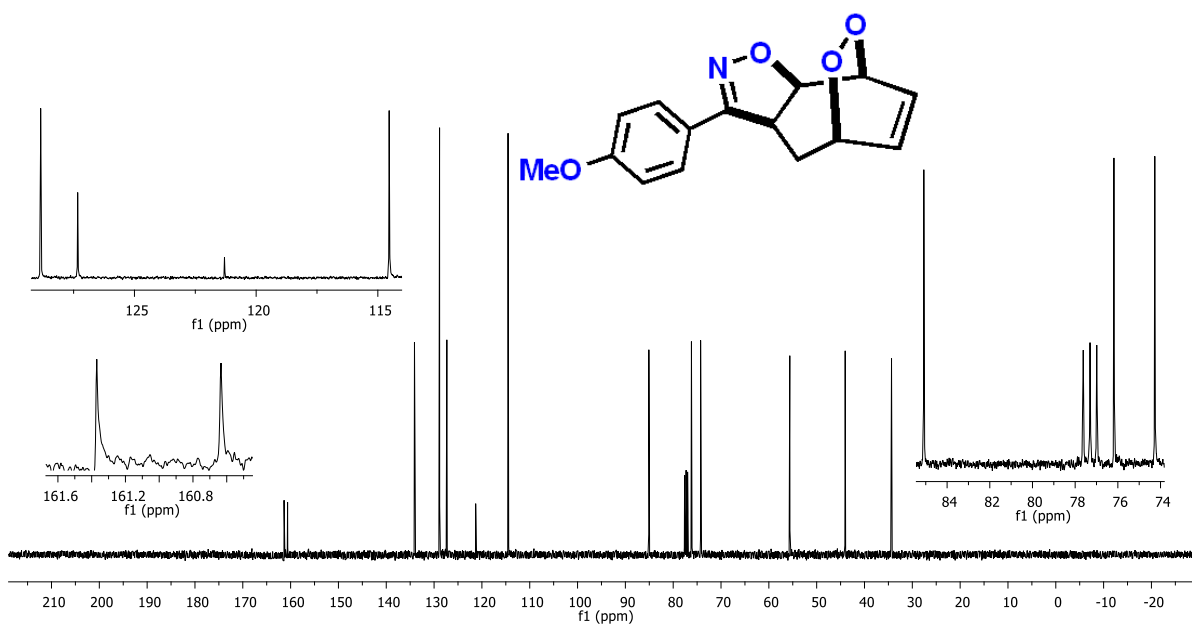
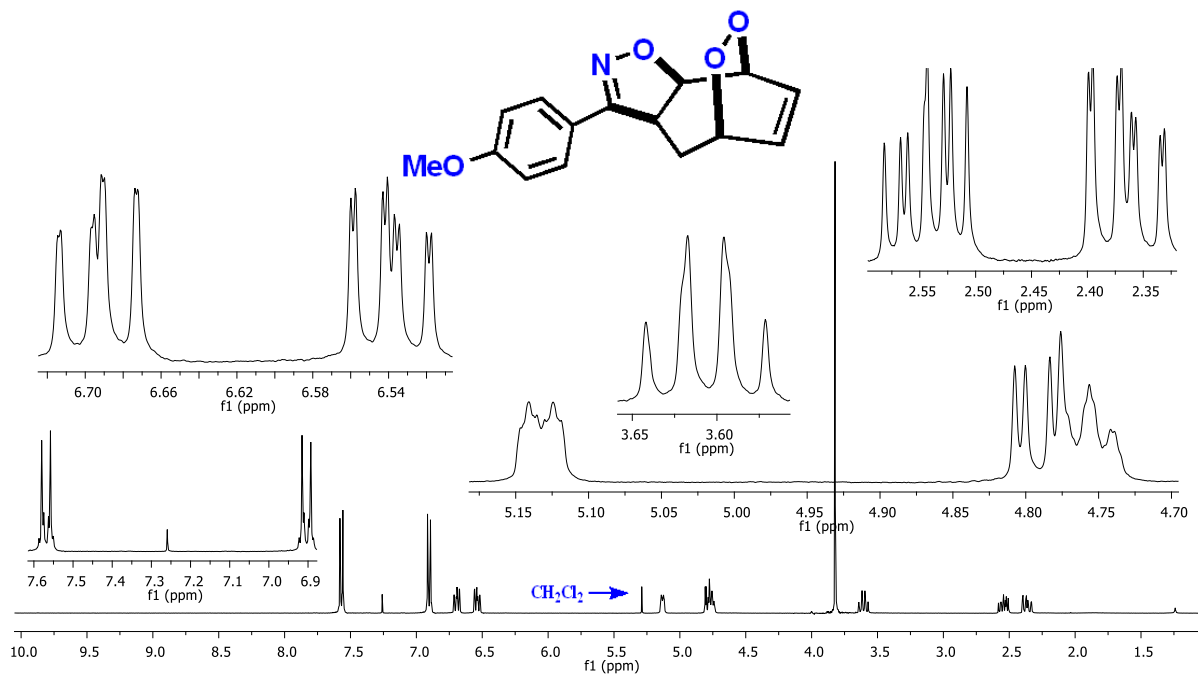


Figure S10. ¹³C-NMR spectrum of **11** (100 MHz, CDCl₃).



HRMS Spectra

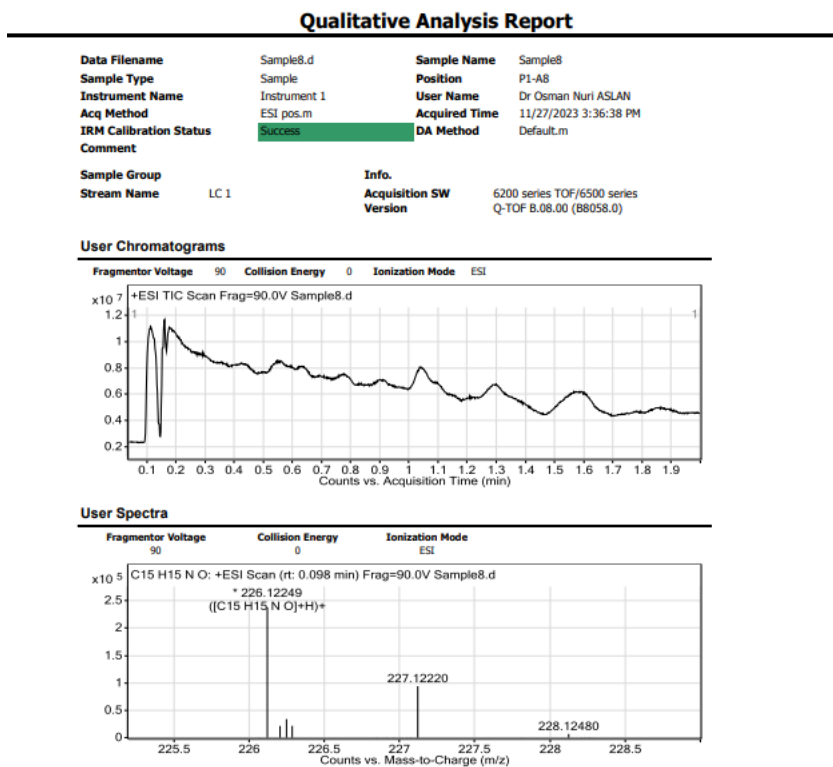


Figure S13. Compound 7.

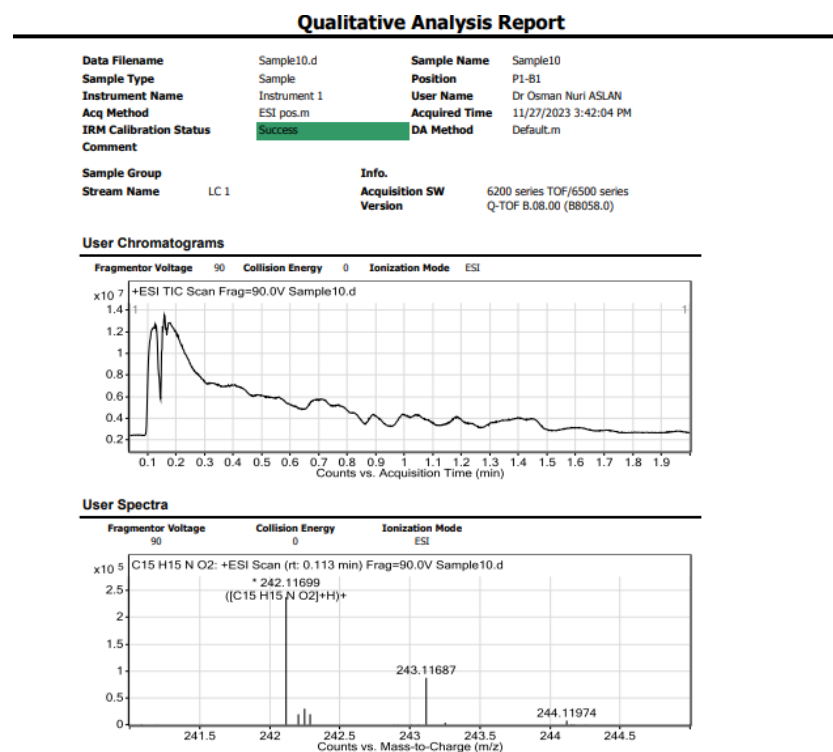
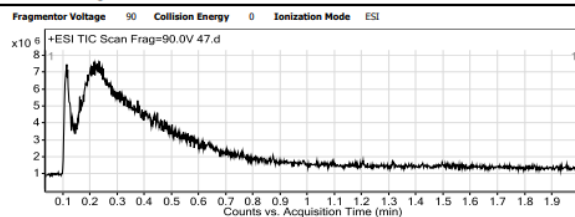


Figure S14. Compound 8.

Qualitative Analysis Report

Data Filename	47.d	Sample Name	47
Sample Type	Sample	Position	p1a2
Instrument Name	Instrument 1	User Name	
Acq Method	ESI pos.m	Acquired Time	11/15/2021 3:20:28 PM
IRM Calibration Status	Success	DA Method	ONA.m
Comment			
Sample Group	LC 1	Info.	
Stream Name		Acquisition SW Version	6200 series TOF/6500 series Q-TOF B.08.00 (B8058.0)

User Chromatograms



User Spectra

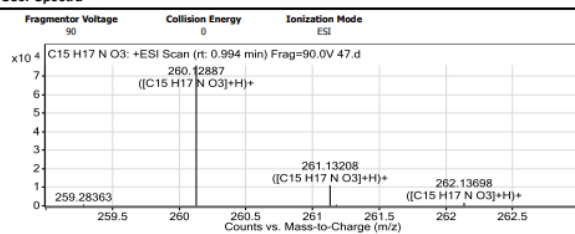
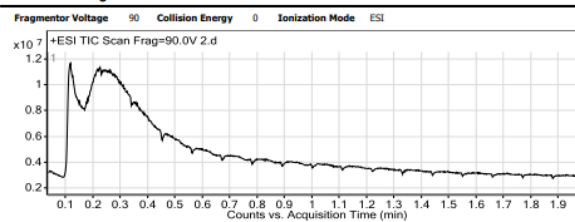


Figure S15. Compound 9.

Qualitative Analysis Report

Data Filename	2.d	Sample Name	2
Sample Type	Sample	Position	p1a2
Instrument Name	Instrument 1	User Name	
Acq Method	ESI pos.m	Acquired Time	10/10/2023 11:26:50 AM
IRM Calibration Status	Success	DA Method	Default.m
Comment			
Sample Group	LC 1	Info.	
Stream Name		Acquisition SW Version	6200 series TOF/6500 series Q-TOF B.08.00 (B8058.0)

User Chromatograms



User Spectra

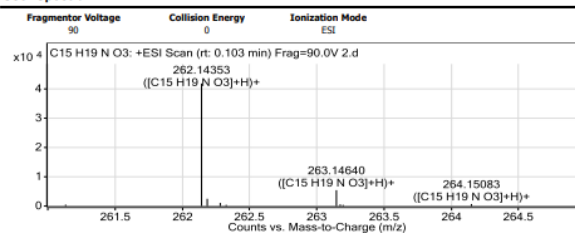


Figure S16. Compound 10.

Qualitative Analysis Report

Data Filename	Sample6.d	Sample Name	Sample6
Sample Type	Sample	Position	P1-A6
Instrument Name	Instrument 1	User Name	Dr Osman Nuri ASLAN
Acq Method	ESI pos.m	Acquired Time	12/22/2023 1:14:57 AM
IRM Calibration Status	Success	DA Method	Default.m

Sample Group		Info.	
Stream Name	LC 1	Acquisition SW Version	6200 series TOF/6500 series Q-TOF 10.1 (48.0)

User Spectra

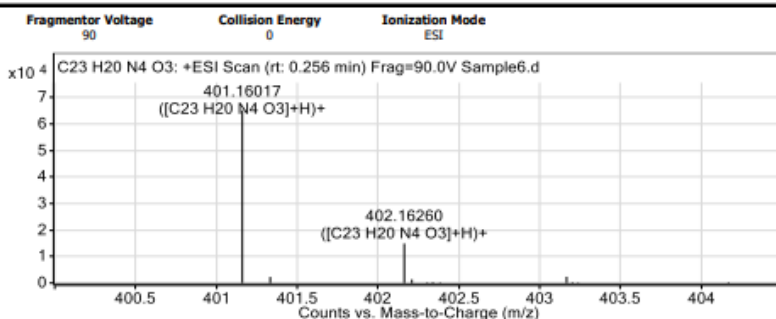


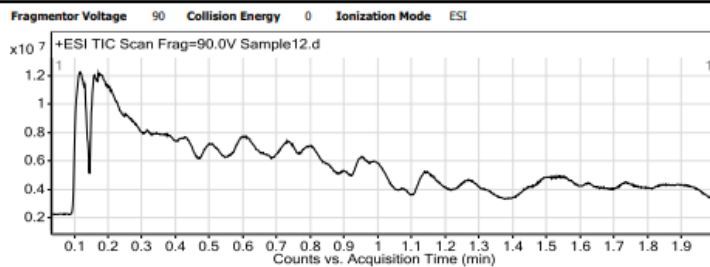
Figure S17. Compound 11.

Qualitative Analysis Report

Data Filename	Sample12.d	Sample Name	Sample12
Sample Type	Sample	Position	P1-B3
Instrument Name	Instrument 1	User Name	Dr Osman Nuri ASLAN
Acq Method	ESI pos.m	Acquired Time	11/27/2023 3:47:27 PM
IRM Calibration Status	Success	DA Method	Default.m

Sample Group		Info.	
Stream Name	LC 1	Acquisition SW Version	6200 series TOF/6500 series Q-TOF B.08.00 (B8058.0)

User Chromatograms



User Spectra

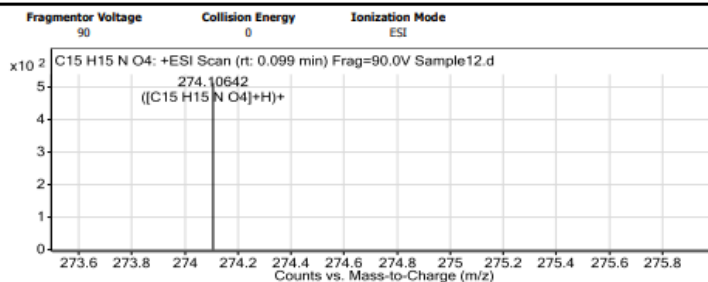


Figure S18. Compound 12.

Cartesian coordinates for the optimized structures (M06-2X/6-311+G(d,p)

Structure no.: TS1

	X	Y	Z
C	-3.38283900	-1.70266400	-0.15088600
C	-2.31430200	-1.76490500	0.72578200
C	-1.11463000	-0.87214800	0.79238600
C	-0.77838800	-0.13255800	-0.50552900
C	-1.78746700	0.93179200	-0.89341400
C	-3.25301500	0.68902500	-0.77711100
C	-3.86140400	-0.52994100	-0.78274200
C	0.38932500	0.79997500	-0.23667000
N	0.01271100	2.00195500	-0.01113500
O	-1.36955500	2.09183900	-0.15298800
C	1.79671000	0.39181700	-0.11586400
C	2.18740100	-0.90367700	-0.45330600
C	3.51904700	-1.29369100	-0.33510600
C	4.48956100	-0.40426400	0.11896300
C	4.08917600	0.89556600	0.45717300
C	2.76817100	1.29118200	0.34509800
C	5.93264000	-0.81217900	0.24739100
H	-4.05266300	-2.55542500	-0.15268400
H	-2.23783800	-2.68041700	1.30385300
H	-0.25609400	-1.47151300	1.10446300
H	-1.27309700	-0.11883000	1.57270200
H	-0.59802300	-0.82548000	-1.32785800
H	-3.85711700	1.55404600	-1.03644800
H	-4.90531200	-0.55690100	-1.08004700
H	1.45701000	-1.61859300	-0.81562800
H	3.80324900	-2.30539600	-0.60339900
H	4.82989700	1.60225800	0.81744100
H	2.47336600	2.29788100	0.61561800
H	6.56607800	-0.19464000	-0.39403900
H	6.28186900	-0.68086400	1.27414900
H	6.07541400	-1.85585800	-0.03302600
H	-1.62121200	1.17594700	-1.95581200
O	-3.45335700	0.56728400	1.63553500
O	-3.51440000	-0.62919100	1.97938900

Structure no.: RC (7+ ¹O₂)

	X	Y	Z
C	-3.33418100	-1.39766700	-1.00301300
C	-2.16495400	-1.83119500	-0.50130600
C	-1.14489200	-0.94116500	0.13704300
C	-0.68334300	0.18011900	-0.81216400
C	-1.67056500	1.33478300	-0.92285300
C	-3.14060400	1.11269400	-0.79486300
C	-3.83276500	-0.03056300	-0.91915000
C	0.47082700	0.94177700	-0.18837100
N	0.10680100	2.04727500	0.33991300
O	-1.25234900	2.24111200	0.12856700
C	1.85269100	0.44810200	-0.08530300
C	2.24049300	-0.70679500	-0.76415200
C	3.54702500	-1.17912600	-0.66656000
C	4.49436100	-0.51424500	0.10767900
C	4.09718000	0.64431400	0.78821600
C	2.80088100	1.12054500	0.69787200

C	5.90960300	-1.01462800	0.22078700
H	-4.01731600	-2.12812300	-1.42453300
H	-1.93755400	-2.89043300	-0.56816100
H	-0.28522300	-1.52768500	0.46438200
H	-1.56669500	-0.45583100	1.02792500
H	-0.43551500	-0.22026200	-1.79527700
H	-3.70504300	2.03632200	-0.69878000
H	-4.91568900	0.06172100	-0.93351400
H	1.52741300	-1.24763800	-1.37623700
H	3.82946400	-2.07842500	-1.20298400
H	4.82008700	1.17444600	1.39976800
H	2.50836400	2.01492500	1.23470100
H	6.61345800	-0.27337300	-0.16537600
H	6.17118100	-1.20089700	1.26506600
H	6.04715100	-1.94064900	-0.33766000
H	-1.48689000	1.86201700	-1.87016500
O	-3.79761000	-0.31107200	1.94951600
O	-3.77070900	-1.49488300	1.77670200

Structure no.: Compound 9 (PC)

	X	Y	Z
C	-3.25295500	-1.72887500	-0.60833100
C	-2.45377600	-1.64061300	0.66807800
C	-1.02737500	-1.08554900	0.51945100
C	-0.81557500	-0.06374800	-0.62257900
C	-1.89104200	1.00966600	-0.83850600
C	-3.28511000	0.66793300	-0.32349400
C	-3.74129500	-0.57411000	-1.04495700
C	0.34505500	0.85030700	-0.29297800
N	-0.01182100	2.04818200	-0.02785400
O	-1.38840400	2.17642100	-0.16795400
C	1.74807300	0.42118400	-0.17542100
C	2.16132700	-0.79422400	-0.72023100
C	3.48743800	-1.20422900	-0.60872600
C	4.42875300	-0.41647400	0.04935700
C	4.00615300	0.80268800	0.59512300
C	2.69009300	1.21807300	0.48878600
C	5.86349500	-0.85212700	0.18293200
H	-3.47037300	-2.68513600	-1.06785000
H	-2.42288800	-2.59934400	1.18750500
H	-0.34310500	-1.92051900	0.35662700
H	-0.76238100	-0.63910400	1.48164500
H	-0.64961300	-0.59829700	-1.55809300
H	-3.95756900	1.51109900	-0.48975400
H	-4.39566700	-0.47757800	-1.90211000
H	1.45311700	-1.42730900	-1.24297700
H	3.79106700	-2.15219300	-1.03955500
H	4.72390700	1.42776200	1.11641600
H	2.37474200	2.15885400	0.92375600
H	6.53184400	-0.13479800	-0.29937300
H	6.15278400	-0.91091100	1.23490200
H	6.02381300	-1.82975000	-0.27222600
H	-1.96020900	1.24679600	-1.90657600
O	-3.21935400	0.52710900	1.10979300
O	-3.21552600	-0.82431000	1.56586300

Structure no.: TS1'

		X	Y	Z
C	-1.44345500	-1.32141400	1.31349200	
C	-1.20076400	-1.77189000	0.04076800	
C	-1.14919400	-0.99900300	-1.24028000	
C	-1.06379600	0.51641100	-1.16509900	
C	-2.22403700	1.25596400	-0.51617300	
C	-2.73992900	0.74001300	0.80319300	
C	-2.18066800	-0.15894000	1.65943200	
C	0.06949500	1.15721400	-0.38206300	
N	-0.26330200	2.28652800	0.11225700	
O	-1.61350500	2.52970500	-0.17847200	
C	1.42852600	0.62078700	-0.21286700	
C	2.07015200	-0.04316000	-1.26055300	
C	3.36058400	-0.53263900	-1.09391400	
C	4.03547700	-0.38523400	0.11879000	
C	3.38507200	0.28069300	1.16200500	
C	2.09895500	0.77681200	1.00371400	
C	5.41648900	-0.95310500	0.31184400	
H	-1.24827600	-2.01893700	2.12083900	
H	-0.84029500	-2.79287600	-0.04245800	
H	-2.02521200	-1.26592700	-1.84028000	
H	-0.28909500	-1.37328400	-1.80067700	
H	-0.97109800	0.88806600	-2.19372100	
H	-3.48705200	1.40784700	1.22367500	
H	-2.52900800	-0.12511400	2.68730200	
H	1.57688000	-0.15207300	-2.22018400	
H	3.85219000	-1.03391100	-1.92087500	
H	3.89306600	0.40705900	2.11241000	
H	1.59898100	1.28092000	1.82265300	
H	6.02838700	-0.29634500	0.93222200	
H	5.36292100	-1.92410200	0.81213900	
H	5.91974200	-1.09792600	-0.64470700	
H	-3.04263800	1.46730700	-1.20137300	
O	-3.36277200	-2.09397300	-0.07308200	
O	-3.91545100	-0.99466400	-0.23425800	

Structure no.: RC' (7+ ¹O₂)

		X	Y	Z
C	-1.57520400	-1.02424100	1.33010200	
C	-0.97590200	-1.43727900	0.20112200	
C	-1.19311400	-0.81145100	-1.14376900	
C	-0.95338200	0.70239700	-1.17658500	
C	-2.08503500	1.55375000	-0.60274100	
C	-2.87650100	1.01151500	0.56136300	
C	-2.59769400	0.01071900	1.41318400	
C	0.19221200	1.24639300	-0.34568000	
N	-0.07992300	2.36529300	0.20451300	
O	-1.38958000	2.73189400	-0.10972900	
C	1.51224300	0.61898300	-0.18627100	
C	2.05072000	-0.16728200	-1.20658900	
C	3.30658200	-0.74557900	-1.05857200	
C	4.04811800	-0.56596700	0.10962500	
C	3.49980200	0.22077700	1.12707200	
C	2.24926300	0.80483100	0.98678600	

C	5.39021100	-1.22637800	0.28281000
H	-1.36001500	-1.55427900	2.25203000
H	-0.28244600	-2.27011900	0.25931900
H	-2.23075500	-0.97889600	-1.46394300
H	-0.55958300	-1.30308700	-1.88113800
H	-0.77883200	1.00696800	-2.21517400
H	-3.72620600	1.64051700	0.81303600
H	-3.25164200	-0.07241600	2.27779700
H	1.50307600	-0.30972100	-2.13161600
H	3.71774400	-1.34348100	-1.86495600
H	4.05998300	0.37249500	2.04380000
H	1.82931500	1.40307100	1.78670600
H	6.04567600	-0.62397600	0.91331000
H	5.27646300	-2.20383300	0.76006400
H	5.87858500	-1.38196400	-0.68010100
H	-2.76540100	1.90810800	-1.37636800
O	-3.48667200	-2.56643000	0.03765400
O	-4.21755000	-1.66465900	-0.26236300

Structure no.: Compound 9' (PC')

	X	Y	Z
C	-1.40426600	-1.04548000	1.44662100
C	-1.68555100	-1.82340900	0.18740800
C	-1.09274600	-1.21146500	-1.08908500
C	-1.04657200	0.32390900	-1.19275000
C	-2.26286200	1.11292300	-0.69113400
C	-3.03707800	0.42847800	0.44801200
C	-2.13304500	0.05367100	1.59173100
C	0.03562200	1.04323400	-0.40493900
N	-0.34863000	2.15063900	0.09390400
O	-1.70769500	2.34040900	-0.18489700
C	1.42004000	0.57601900	-0.22859400
C	2.08985700	-0.07613400	-1.26627400
C	3.40154100	-0.50244100	-1.09570100
C	4.07160300	-0.30329500	0.11273200
C	3.39268500	0.34800700	1.14672900
C	2.08453000	0.78172300	0.98376600
C	5.47822500	-0.80184400	0.31221800
H	-0.70141000	-1.40820700	2.18673200
H	-1.36161400	-2.86173500	0.27210200
H	-1.66786100	-1.60667200	-1.92951400
H	-0.07484700	-1.59067700	-1.19917600
H	-0.87264100	0.56617700	-2.24738300
H	-3.83020700	1.10160700	0.77808400
H	-2.08776800	0.69923500	2.45978400
H	1.59470500	-0.23388900	-2.21866100
H	3.91295700	-0.99690900	-1.91474000
H	3.89610500	0.51246600	2.09373700
H	1.56381200	1.27674100	1.79541200
H	6.06084900	-0.10257700	0.91408800
H	5.47227300	-1.76187200	0.83586200
H	5.98435400	-0.94550300	-0.64291400
H	-2.95919800	1.36969500	-1.48891500
O	-3.10850300	-1.95982100	0.08727000
O	-3.72892700	-0.69255500	-0.14190600